A Hand-Held Non-Robotic Surgical Tool with a Wrist and an Elbow

Katherine E. Riojas[1], *Student Member, IEEE*, Patrick L. Anderson[1], *Student Member, IEEE*, Ray A. Lathrop[1], S. Duke Herrell[1], D. Caleb Rucker[2], *Member, IEEE*, and Robert J. Webster III[1], *Senior Member, IEEE*

***Abstract*—*Objective:* This paper describes a surgical device that provides both wrist and elbow dexterity without motors or electronics. The device provides dexterity advantages in minimally invasive surgery typically associated with robotic systems, but does so with many fewer components. Fully mechanical designs of this type promise to deliver "robot-like dexterity" at a lower financial cost than current surgical robotic systems. *Methods:* Most non-robotic articulated surgical tools developed to date feature one or two degrees of freedom (DOF) close to the tool tip (i.e. a "wrist"). In this paper, we describe a new tool that not only features a two-DOF wrist, but augments its dexterity with a two-DOF "elbow" consisting of a multi-backbone design seen previously only in robotic systems. Such an elbow offers high stiffness in a thin form factor. This elbow requires static balancing, which we accomplish with springs in the handle so that the surgeon can benefit from the stiffness without feeling it while using the device. *Results:* We report the overall tool design and experiments evaluating how well our static balance mechanism compensates for the multi-backbone elbow's intrinsic stiffness. *Conclusion:* We demonstrate use of a multi-backbone elbow in a manual tool for the first time and show how to combine the elbow with a pin joint wrist in a fully mechanical (i.e. non-robotic) tool. *Significance:* This work is a step toward high dexterity, low-cost surgical instruments that bring some benefits of surgical robotic systems to patients and surgeons at a lower cost.**

***Index Terms*—Medical Devices, Minimally Invasive Surgery, Surgical Robotics**

I. Introduction

THE benefits of minimally invasive surgery (MIS) for the patient (e.g. shorter hospital stays, reduced pain, etc. [1], [2]) have motivated its adoption, despite the fact that it increases the challenge of performing a variety of surgical maneuvers for the surgeon [3]. Returning dexterity to the surgeon has been one of the key motivators of wide deployment of robotic surgical systems over the past few years [4], [5].

Traditional manual MIS tools consist of a long, straight, rigid shaft that connects a set of jaws to a handle. When inserted into the body, the rigid shaft results in a cone-shaped workspace that requires a substantial amount of free space inside the patient. This workspace requirement explains why initial MIS procedures were performed in the abdomen, which can be insufflated to create the requisite space.

The desire for wrist dexterity was one of the key motivators in the development of robots like the da Vinci® Surgical System that made minimally invasive surgeries much easier to perform [4], [6]. As robots push forward into new applications in deep, narrow spaces like the throat [7] and colon [8], [9], additional degrees of freedom are needed, and many of the robots developed for such spaces feature continuously bending (i.e. "continuum" structures).

It has previously been noted that it would be desirable to create dexterity analogous to the da Vinci and other robotic systems in hand-held non-robotic packages to reduce the high cost of current surgical robotic systems [3], [5], [10]. For example, Diks et al. created a fully mechanical analogue to the da Vinci that attaches to the patient's bed [11]. By eliminating the motors, sensors, computers, and other equipment inherent to robotic systems, non-robotic articulated surgical tools have the potential to provide dexterity for the physician in an inexpensive manner. A non-robotic dexterous tool also eliminates the need to re-engineer the surgical workflow, as must be done when the surgeon sits at a console and does not physically interact with the patient [2], [4].

Several review papers have surveyed the existing hand-held articulated mechanical tools that have been on the commercial market or are under development in research laboratories [3], [10], [12], [13], [14]. Broadly speaking, these tools typically include a shaft, a control handle, and two distal degrees of freedom (i.e. a "wrist") coupled via cables or mechanical linkages to a surgeon control handle. The distal wrist degrees of freedom can be provided through a variety of mechanisms: most common are pin joints (e.g., [6]) and continuum joints (e.g., Medtronic SILS™ Hand Instruments). Researchers at Delft University of Technology have developed several manual instruments with wrist-like dexterity using both rolling joints (DragonFlex) and innovative continuum joints (I-Flex) [15], [16]. Another novel dexterous manual tool was developed by Awtar et al. called the FlexDex™ [17]. These devices incorporate a wrist joint (adding two DOF) and a gripper (adding one DOF).

This work was supported by the National Science Foundation Graduate Research Fellowship Program under Grant No. DGE-1445197, as well as by the National Institutes of Health in part by the National Institute of Biomedical Imaging and Bioengineering training grant T32EB021937. Any opinions, findings, and conclusions or recommendations expressed in this material are those of the authors and do not necessarily reflect the views of the National Science Foundation or the National Institutes of Health.

[1]Authors are with the Department of Mechanical Engineering and the Vanderbilt Institute for Surgery and Engineering (VISE), Vanderbilt University, Nashville, TN, USA (e-mail: katherine.e.riojas, patrick.l.anderson, ray.lathrop, duke.herrell, robert.webster@vanderbilt.edu), S. D. Herrell and R. J. Webster III are also with the Department of Urologic Surgery, Vanderbilt University Medical Center, Nashville, TN, USA. [2]D. C. Rucker is with the Department of Mechanical Engineering, University of Tennessee, Knoxville, TN, USA (e-mail: drucker6@utk.edu)

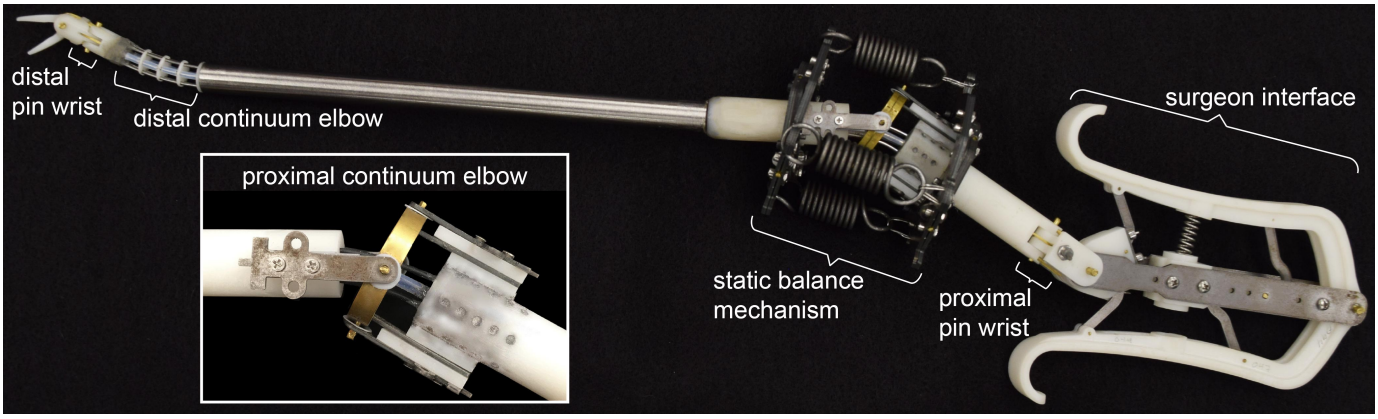

Fig. 1: The tool described in this paper combines a pin joint wrist with a multi-backbone continuum elbow. The distal wrist is connected by pull-wires to a mirror image pin joint in the tool handle. As the surgeon applies an angular deflection to the surgeon interface, the wrist tilts in a corresponding direction. The pull-wires run through hollow tubes in a distal multi-backbone continuum elbow, as well as a proximal elbow. As the proximal elbow is deflected (see inset), tension and compression are transmitted along the nitinol tubes within the tool shaft to the distal elbow, causing it to deflect. Together, these two elbows are stiff and would be difficult to bend by hand during surgery. An over-center spring static balance mechanism surrounds the proximal elbow and compensates for the stiffness of both elbows.

The addition of wrist DOF is useful in enabling the tool to approach the surgical site from a variety of angles, or for restoring wrist-like dexterity to the surgeon for performing complicated motions such as suturing. However, the instrument shaft still requires an open, approximately cone-shaped workspace inside the patient similar to that required for traditional MIS instruments. This requirement creates challenges when performing surgery in deep, narrow anatomical spaces in the human body (e.g., the throat, upper airways, and colon) where tool shafts are constrained to small angular deflections by the geometry of the deep cavity.

These challenges motivate adding additional degrees of freedom to dexterous manual tools. In this paper, we define an "elbow" as any mechanism that provides additional one or two DOF proximal to the wrist (we exclude from consideration grippers or other one-DOF end effectors in this definition, and as mentioned previously, the "wrist" is defined as the distal one or two DOF).

Some of the only existing manual tools that combine wrist and elbow degrees of freedom as defined above were developed by the BITE Group at Delft University of Technology and are the remarkable MultiFlex [10] and HelixFlex [18]. These devices combine multiple continuum sections and so could be considered as having a wrist and then multiple elbows according to our definition above, or as having multiple elbows without a wrist. In the MultiFlex, each elbow is a continuum section created using a collection of pull-wires that are surrounded by an internal and external spring, with one group of pull-wires terminating at each elbow. In the HelixFlex, each elbow is a continuum section created using specific routing of pull-wires that are surrounded by an internal and external spring, with all pull-wires terminating at the same point to increase the ease of manufacturing and miniaturization compared to the MultiFlex. The continuum sections give the devices snake-like dexterity for MIS. Our approach is different in that we use a pin joint wrist which provides large local deflection at the tool tip, and a single continuum elbow that works using push-pull rods rather than tendons with an outer coil spring. Our aim in this paper is not to argue that we have built a better tool than the HelixFlex or MultiFlex, but rather a different one that introduces new mechanisms to the growing family of approaches available to the designer of a fully mechanical articulated tool. Our pin joint wrist, for example, could potentially be added to the MultiFlex or HelixFlex to give them added local tip dexterity. Our multi-backbone elbow offers the potential for higher stiffness than an outer coil spring at the expense of it being more complex to combine multiple elbow sections in a single tool.

In designing a manual tool with an elbow that is both stiff and maneuverable, we drew inspiration from surgical robotics research. The robotics research community has found continuum designs to be useful in creating stiff, yet maneuverable instruments in a thin form factor. Such robots have been designed for performing surgery in deep, narrow anatomical spaces in the human body [19]. Multi-backbone continuum robots in particular have shown great promise in approaching the surgical site along nonlinear paths while still maintaining the ability to apply high forces at the end effector. These multi-backbone structures can be made with elastic wires or tubes as their backbones. An advantage of using tubes is that the lumen of each tube can be used for cable routing for distal wrist actuation, as we do in this paper. Robotically-actuated multi-backbone designs have been studied in detail by Simaan et al. over the past several years [7], [20], [21]. While these robotic systems have proven highly capable, the multi-backbone design has not previously been packaged into a hand-held unit, because the stiff backbones require substantial static actuation forces to remain in a bent configuration – loads easily achieved with robot actuators, but difficult for human hands to apply while at the same time attempting to accomplish accurate surgical maneuvers.

In this paper, we overcome this challenge with a static balance system consisting of springs integrated in the tool handle. This design enables us to combine a stiff multi-backbone continuum elbow with a pinned wrist actuated by pull-wires that pass through the elbow backbones to create a

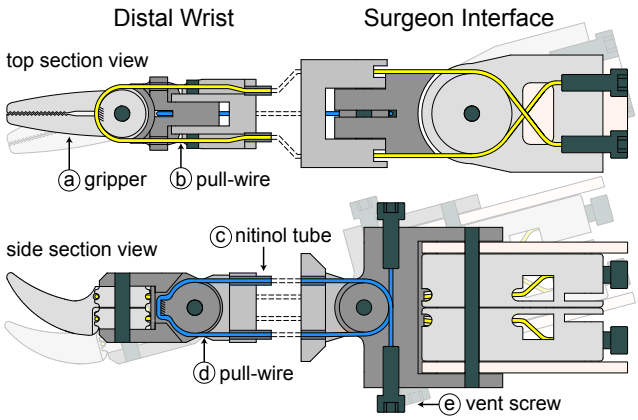

Fig. 2: Schematic views of the pull-wire routing used to actuate the 2-DOF distal wrist. The top section view shows the pull-wire ⓑ that controls one gripper ⓐ. If the surgeon interface is tilted, both jaws move together. If it is squeezed, (i.e., the two surgeon interface levers move toward or away from one another), the jaws open and close. Rotation about an axis perpendicular to pull-wire ⓑ is achieved via pull-wire ⓓ as shown in the side section view. The pull-wires are routed from the distal wrist to the handle through the inner lumens of the nitinol tubes ⓒ that make up the distal and proximal elbows, as shown by the dashed lines. They are secured in the handle and tensioned with vent screws ⓔ.

purely mechanical device with a wrist and an elbow (Fig. 1).

Our compensation system was inspired by a variety of creative compensator designs that have been described previously in the engineering literature [22], [23], [24], but never before been applied to a hand-held surgical tool to counterbalance a multi-backbone continuum section. Our purpose in this paper is to demonstrate the basic feasibility of this tool concept, not to optimize it for any one particular surgical application. The wide variety of clinical scenarios where robots with controllable curved sections have proven useful illustrates the potential for adapting our design to a variety of clinical scenarios, but this is left to future work. Examples include laryngeal surgery as addressed by Simaan et al. [7] and by the Medrobotics Flex® Robotic System [25], as well as the multi-backbone SPORT system for single-port surgery by Titan Medical Inc. [26]. Similarly, Shang et al. describe how curved dexterous robotic tools can be beneficial in transanal surgery, because tools must work in a deep cavity [27]. Thus, there is ample clinical motivation for the dexterity provided by a curved elbow combined with a wrist. In this paper, we explore the feasibility of providing these DOF more simply and inexpensively, without requiring computers and actuators.

II. Device Design

Our design concept is shown in Fig. 1. The design consists of a pin joint wrist connected via pull-wires that run through the tubes of a multi-backbone continuum elbow to a handle. The handle itself contains a copy of the continuum elbow, so that bending motions of the handle can be transferred to tension and compression of the backbones in the distal elbow. The surgeon control interface we use is the same as that previously described by Anderson et al. [6] and has the advantage of being symmetric so that it can be manually rolled within the surgeon's grasp to create axial rotation of the tool. The two multi-backbone elbows are both statically balanced by an over-center spring mechanism surrounding the elbow in the handle. The tip of the tool features a 2-DOF wrist actuated by pull-wires, augmented with jaws for grasping.

A. Wrist and Handle Design

The distal wrist of this tool is coupled to the handle mechanism using three looped pull-wires. The routing of the pull-wires is as shown in Fig. 2. Two pull-wires are looped around separate gripper pulleys, as shown with gripper ⓐ and pull-wire ⓑ in the top section view of Fig. 2. The third pull-wire ⓓ controls the distal wrist rotation by rotating the grippers about an axis perpendicular to the gripper pull-wires, as shown in the side section view. The pull-wire mapping shown in Fig. 2 produces parallel kinematic mapping (i.e. the central axes of the handle and end effector are approximately parallel [6]). All three pull-wires are routed through the inner lumens of the nitinol tubes ⓒ forming the distal and proximal elbows, where they are tensioned with vent screws ⓔ in the surgeon interface. The pull-wires are secured to the distal wrist pulleys with glue.

B. Multi-Backbone Elbows

The continuum, 2 DOF multi-backbone elbows consist of 6 nitinol tubes (1.14 mm OD, 0.96 mm ID) arranged in a 7 mm diameter circle as measured from the tube centers (see Fig. 3). The tubes that form the two elbows are continuous along the length of the shaft to provide mirroring between handle motion and tip motion (see Fig. 1). Tube spacing within the shaft is maintained by a 3D printed insert. Delrin spacing discs are placed along the elbows to support and maintain tube spacing. PTFE sleeves are placed around the tubes between the discs as spacers. The proximal elbow is 20 mm long, and is surrounded by 3 steel springs. A circular ring and rigid link support yoke are positioned coaxially around the proximal elbow (see Fig. 1 inset). The kinematic center of this support structure is located at the midpoint of the elbow to allow the elbow to assume a circular arc as it is deflected. The distal elbow is 25 mm long and has the same 3.5 mm radial tube spacing as the proximal elbow. This constant radial spacing results in a 1:1 ratio between the angle of the proximal elbow and the angle of the distal elbow. The decrease in length of the proximal elbow centerline is equivalent to the increase in length of the distal elbow centerline for a given deflection angle. Thus, if one wished to have something other than a 1:1 ratio (i.e., to build some scaling in between handle motion and tool motion), one could use a different radial spacing on the two elbows. For simplicity, we use a 1:1 ratio in our prototype.

C. Elbow Elastic Energy

As discussed in Section I, we utilized a spring mechanism to statically balance the two elbows. When the user deflects the 2 DOF proximal elbow by one or both of the input angles using the surgeon interface, the nitinol tubes bend and store elastic energy. A restorative torque is generated by the tubes as shown in Fig. 4(a). The spring and gimbal static balance mechanism generates an opposing torque that balances the continuum section torque (Fig. 4(b)).

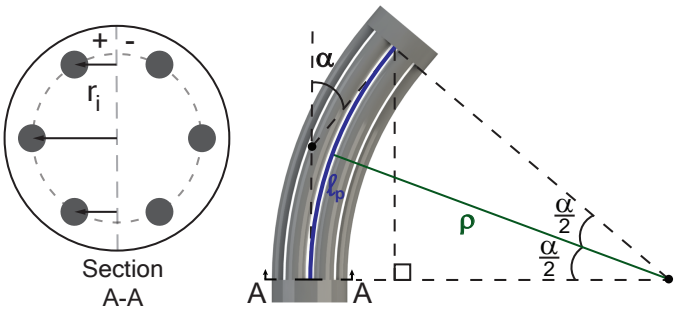

Fig. 3: Planar diagram representing the proximal elbow of the tool. The circular arc has radius of curvature ρ and length ℓ_p, which represents the virtual centerline length of the elbow. α is the articulated angle. When $\alpha = 0$, the elbow is straight and $\ell_p = L_p = 20\,\text{mm}$. When deflected, ℓ_p decreases due to the imposed geometry constraint.

To design the static balance mechanism, we first determined the total strain energy stored in the device. With no external loading, the multi-backbone elbow bends in an approximately constant curvature arc [28], and we assume it to be constant curvature in this work. In an initial configuration when both proximal and distal continuum segments are straight, they have lengths of L_p and L_d respectively. During device operation, we assume each tube has constant total length (no axial compression), such that the length of tube i in the proximal section ℓ_{ip} and its length in the distal section ℓ_{id} are related to each other and to their initial lengths by

$$\ell_{ip} + \ell_{id} = L_p + L_d \qquad i = 1...n. \tag{1}$$

The tube lengths in the distal section are dictated by the coupling of the continuum segments as shown in Fig. 5. The tubes are fixed on either end of the tool (i.e. near the distal tip and near the surgeon interface), but otherwise can slide within the shaft of the device. The rigid link support yoke (shown in green in Fig. 5) holds the shaft of the device fixed relative to the pivot point of the mechanism. The rigid link constraint dictates the decrease in length of the proximal elbow virtual centerline, and since the tubes can slide within the shaft of the device, the distal elbow virtual centerline lengthens by the same amount. The resulting bending relationship of the two multi-backbone joints can be seen in Figs. 1 and 5. Due to the 1:1 ratio of proximal elbow angle to distal elbow angle, the elbows share a common tool axis, and the deflected centerline length of the proximal segment ℓ_p is then a function of the deflection angle α as follows

$$\ell_p = \frac{L_p \alpha}{2\tan(\alpha/2)}. \tag{2}$$

and the individual leg lengths in the proximal section are then

$$\ell_{ip} = \frac{L_p \alpha}{2\tan(\alpha/2)} + r_i \alpha \tag{3}$$

by the constant curvature assumption, where r_i is the normal distance from the centerline to the tube location in the plane of curvature, where positive is away from the bending direction as shown in Fig. 3. Using (1), the distal tube lengths are

$$\ell_{id} = L_p + L_d - \frac{L_p \alpha}{2\tan(\alpha/2)} - r_i \alpha. \tag{4}$$

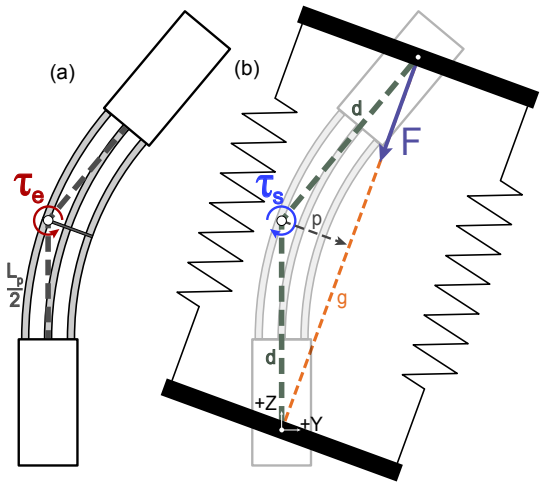

Fig. 4: (a) When the continuum elbow with undeflected length L_p is deflected, a torque τ_e is generated by the tubes to restore the elbow to its straight configuration. (b) The spring mechanism generates a torque τ_s to balance the elbow torque and create a static equilibrium state at the actuation angle. This balancing torque is governed in part by the distance between the gimbal center and support ring center d, the distance between the gimbal centers g when the elbow is deflected, and the resulting moment arm p

Since the distal radial tube spacing is equal to the proximal tube spacing, the length changes described above imply that the distal segment also bends by the same absolute angle α, according to standard constant curvature kinematics. The total elastic energy stored in the distal and proximal segments is then

$$U = \frac{1}{2}\sum_{i=1}^{n}\left(\frac{\alpha^2 EI}{\ell_{ip}} + \frac{\alpha^2 EI}{\ell_{id}}\right) = \frac{1}{2}\alpha^2 k_e, \tag{5}$$

where

$$k_e = EI\sum_{i=1}^{n}\left(\frac{1}{\ell_{ip}} + \frac{1}{\ell_{id}}\right) \tag{6}$$

is the effective torsional spring constant responsible for the restorative torque felt at the handle in Fig. 4, i.e. $\tau_e = \alpha k_e$. Note that this is a nonlinear relationship, as k_e is a function of α through ℓ_{ip} and ℓ_{id} as detailed above.

Assuming that the tube and the wire share the same central axis (i.e. there is a tight tolerance between the pull-wire and the tube that surrounds it), then there will be no effect on tube bending from tensioning the wire, regardless of tube bend angle. This lack of influence is because the tension is always

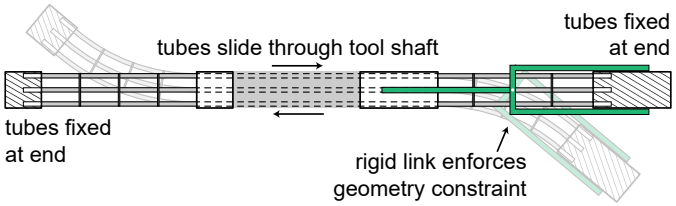

Fig. 5: Schematic of relationship between the elbow joints. The rigid link support yoke (shown in green) holds the shaft of the device fixed relative to the pivot point. The tubes are fixed at each end (near the distal tip and near the surgeon interface), but are free to slide throughout the shaft of the device. The rigid link constraint dictates the centerline length change of the proximal elbow centerline. Since the tubes slide freely through the tool shaft before connecting to the distal tip, the virtual centerline length of the distal segment lengthens by the same amount.

directed axially along the tube and the bending moment is not a function of wire tension. To understand this concept, consider an arbitrary cross section of a nitinol tube with a wire routed through it as a free body. Since the wire and tube share the same central axis, the wire tension does not appear in the moment balance of the tube. Similarly, consider the entire distal portion of the elbow with the wires routed through the nitinol tubes as a free body. Summing the moments about the center of the tube at this cross section, one can see that wire tension again does not affect the internal moment of the tube, since it does not appear in the moment balance. Thus, the only effect of the wire tension is to increase the internal force that is axially compressing the tubes. In practice, this compression is so small that it is negligible because the tubes have high axial stiffness relative to their bending stiffness.

This analysis assumes zero clearance between the tube inner wall and the outer surface of the wire. In practice, there will be a very small clearance, causing small backlash between the wire and tube. However, this effect is small for a close tolerance, which we have in our prototype, and so it is neglected in this paper.

D. Static Balance Mechanism

An over-center spring mechanism was selected as the method of compensation for this design. This design features two steel gimbals positioned coaxially around the proximal elbow with 3 springs attached between them. The gimbals are located $50\,\text{mm}$ apart from one another along the tool axis when the elbows are straight and each consists of 3 concentric steel plates (see Fig. 1). The outer gimbal plates always remain parallel to one another during operation due to the symmetric nature of the design.

Since the outer gimbal plates are parallel, the length of each of the springs is the same for a given set of deflection angles and each spring will exert the same force. These three equal forces can be simplified to a single equivalent force acting between the center of the top gimbal and the center of the bottom gimbal (see Fig. 4). The vector $\boldsymbol{g}$ between the two gimbal centers is given by

$$\boldsymbol{g} = \begin{bmatrix} d\cos(\gamma)\sin(\beta) \\ -d\sin(\gamma) \\ d + d\cos(\gamma)\cos(\beta) \end{bmatrix} \tag{7}$$

for a rotation γ about the positive X-axis and then rotation β about the positive Y-axis, where d is the distance between a gimbal center and the center of the support ring. We can then find the perpendicular distance from the center of the support ring to the line connecting the two gimbal centers (see Fig. 4). This perpendicular distance p is given by

$$p = \sqrt{d^2 - \frac{g^2}{4}}, \tag{8}$$

where g is the norm of $\boldsymbol{g}$ from (7). To allow the use of stock manufactured springs that are only available in specific lengths, small inextensible wire links were used to attach the springs to the gimbals. The length σ of these links changes the initial spring length, and allows for fine adjustment of the compensation torque provided by the springs. It should be noted that the unstretched length of the selected springs is shorter than the distance $2d-\sigma$. Because of this, a base spring tension is required to attach the springs to the inextensible links. As a result, the spring is extended even when the elbow is undeflected. We denote the unstretched length of the spring without this pretension as c.

Finally, the total force generated by all three springs of the static balance mechanism is the combination of the minimum force to start to extend the spring b and the force due to the change in spring length. Using the spring constant k, the resulting torque τ_s is given by

$$\tau_s = 3(k(g - \sigma - c) + b)p. \tag{9}$$

E. Selection of Components

After characterizing the restorative torque from the elbows τ_e and spring compensation torque τ_s, we selected design parameters to minimize the difference in these two torques throughout the tool's range of motion. As shown in the torque curves of Fig. 6, the net torque resulting from the compensation becomes increasingly nonlinear as the deflection angle increases. We designed our tool for a maximum bend angle of 30° in each direction. This number was selected somewhat arbitrarily for our prototype to provide a qualitatively good trade-off between maximum bend angle and torque linearity.

Design parameters for the elbows include number of tubes composing each elbow, the tube dimensions, the radial spacing of the tubes, and the total length of the undeflected elbows. The tube dimensions were selected first based on available nitinol stock, while the radial spacing and elbow lengths were chosen to create a stiff elbow in a relatively small form factor while maintaining a 1:1 ratio of input to output angles. These values are given in Section II-B.

The torque of the elbows τ_e is approximately linear; however, the torque of the compensation mechanism τ_s is nonlinear as shown in Fig. 6. Spring compensation parameters include yoke length d, the number of springs (so long as they are symmetric), spring stiffness k, unstretched length c, minimum load b, and offset length σ. The distance d between one of the gimbal's centers and the center support ring including gimbal thickness was selected to be $2.67(L_p/2)$ to keep the size of the compensation mechanism small but still have a suitably large moment arm p for compensation. We used 3 springs for design simplicity, since this is the minimum number of springs to provide effective compensation for the 2 DOF elbow with our design based on the assumption of an equivalent spring force between the gimbal centers.

After selecting the aforementioned parameters, the uncompensated experiments described in Sec. III-A were performed to determine the elastic modulus of the multi-backbone elbows. Using a linear regression of the experimental torque data of the uncompensated system, the modulus was found to be approximately $42\,\text{GPa}$. Using (6), we calculated the elbow torque τ_e and selected stock music-wire steel extension springs ($k = 4466\,\text{N/m}$, $c = 38.1\,\text{mm}$, $b = 7.56\,\text{N}$) to provide the correct spring compensation torque, τ_s. Finally, we refined the spring compensation torque by adjusting the inextensible offset length σ, which changes the initial stretched length of

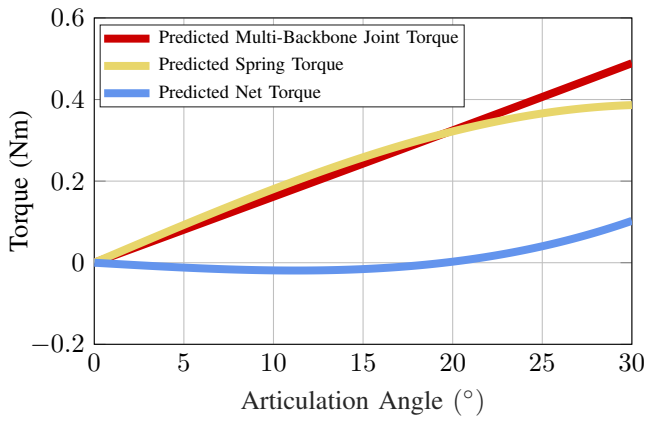

Fig. 6: Predicted theoretical torque curves for the elbow tool, shown over a range of input articulation angles. The multi-backbone elbow joint torque is shown in red , the compensation mechanism torque is shown in yellow , and the net torque is shown in blue . The net torque is close to zero through the first 20 degrees of articulation, after which the nonlinearity of the spring compensation torque results in a small torque felt by the user.

the spring. After comparing the spring torque and elbow torque throughout the tool range of motion, we selected an offset of 11 mm to achieve this goal.

III. Experiments

A. Joint Actuation Test

To measure the effectiveness of our static balance mechanism in compensating for the stiffness of the two elbows, we performed a deflection-force test both with and without the spring compensator in place (see Fig. 7). A force perpendicular to the tool shaft was applied to the device handle 48.5 mm away from the center of the proximal elbow as measured with 0° of articulation. We created a double-pin attachment (see Fig. 7 inset) that allowed both pushing the elbow to its maximum deflection angle and also pulling it back to its undeflected position by applying a force only at a point. In other words, this attachment allowed push-pull actuation of the joint without adding an undesirable reaction moment to the system. For each test, force was applied in four directions: the positive and negative x-axis and the positive and negative y-axis according to the coordinate frame shown in the Fig. 7 inset. The tool was rotated in the chuck between tests to achieve these four tool orientations. Three trials were performed in each orientation for a total of twelve trials.

Force data was obtained with a 6-axis ATI Mini force sensor (ATI Industrial Automation, Apex, NC). Linear displacement was generated using a linear slide. Force data was recorded for every two millimeters of load cell travel and this displacement was used to calculate the effective lever arm (the perpendicular distance between the location of the applied force and the center of the proximal elbow). Planar motion of the elbow was assumed, and the total force was calculated as the norm of the measured forces in the plane of the linear slide.

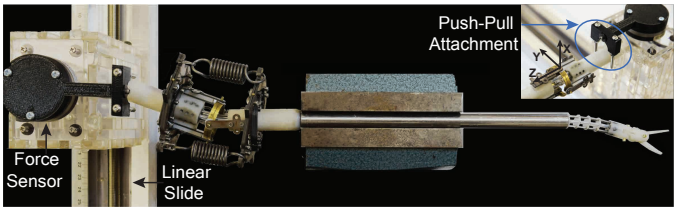

Fig. 7: The apparatus used for verifying elastic compensation, which consists of a linear slide for deflecting the handle and a force sensor for measuring the torque required to do so. The force required to deflect the elbows was measured with and without the elastic compensator in place.

Fig. 8(a) shows twelve trials of the uncompensated and compensated performance of the device. Fig. 8(b) shows the average experimental data and theoretical torque predicted by our model on the same graph. The standard deviation of the experimental results is overlaid on these same plots as a shaded region about the average. The uncompensated elbows required a maximum of 0.55 Nm to generate 30° of deflection. This includes the torque needed to overcome both the modeled elastic and unmodeled frictional forces. The compensated system had a consistently lower actuation torque requirement, requiring a maximum torque of only 0.21 Nm to actuate the joint. In the joint actuation test, hysteresis (which is likely due to frictional effects) constituted a maximum of 0.09 Nm in the uncompensated case and a maximum of 0.15 Nm in the compensated case.

B. Distal Elbow Stiffness

One of the advantageous features of this device is the high stiffness of the multi-backbone joint. We experimentally measured the stiffness of the elbow by fitting a line to the x-axis deflection of the backbone centerline vs. the applied force in the -x direction as defined by the coordinate system in Fig. 7 without the compensator present. We hung 8 different weights directly behind the distal pin joint with magnitudes ranging from 0 g to 700 g spaced in 100 g increments. The measured stiffness at the end effector was 3.7 N/mm when the handle was locked in its equilibrium (straight) position. Repeating this same experiment with the handle rotated to near the midpoint of full deflection (−13°) about the y-axis in the x-z plane resulted in a measured stiffness of 2.3 N/mm. Repeating for when the elbow is rotated 13° about the y-axis resulted in a measured stiffness of 3.4 N/mm.

C. Peg Transfer Task

In this section, we performed a peg transfer user study to investigate dexterity through a constrained lumen using three different devices. Such a scenario would occur in surgery when performing a procedure in a deep, narrow access path, as would occur in throat surgery or transanal colon surgery. We compared the performance of a traditional rigid laparoscopic tool, a tool with a wrist only [6] (where the wrist is kinematically identical to the one described in this paper), and the tool described in this paper that has both a wrist and an elbow. In this experiment, the user (an author of this paper - Anderson) was asked to complete a peg transfer task, in which rings are moved from one peg to another on a peg board with all three tools. The peg board had 15 pegs and the user's task was to transfer a rubber ring from a peg on one side of the board to its corresponding mirror image peg on the opposite side of the board. The user had no previous surgical experience,

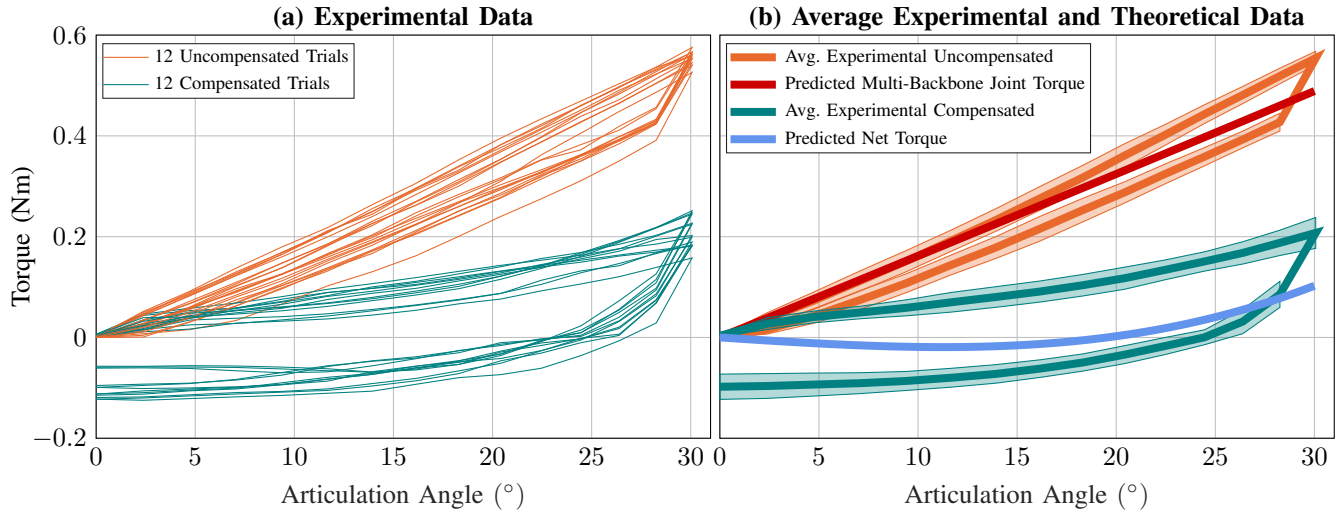

Fig. 8: (a) Twelve trials of the torque of the proximal elbow in the uncompensated configuration are shown in orange and in the compensated configuration in green . (b) Comparison of average torque felt in the uncompensated and compensated configuration with the theoretical curves overlaid. The standard deviation is shown in the shaded region above and below each of the average experimental curves. The red line shows the predicted multi-backbone torque τ_e. The blue line shows the predicted compensated net torque curve generated from the difference in the predicted elbow torque τ_e and the spring compensation torque τ_s.

other than a user study in [6]. The purpose of this experiment was to evaluate whether the new device could enable the user to reach previously inaccessible locations while performing a task. Failures can be viewed at the top of Fig. 9 as black rings. Successful transfers are shown using filled blue dots. From the figure, one can see that the standard and wristed tools performed similarly in this particular task, and were not able to reach the outermost column of pegs at all, even with full instrument tilt in the constrained lumen. In contrast, the elbow tool was able to successfully reach all of the target pegs. This experiment demonstrates that the elbow tool enabled the user to perform a task that was not possible without the larger workspace enabled by the inclusion of the multi-backbone elbow.

One specific situation in which this increase in interior workspace might be beneficial would be in central airway obstruction removal surgery. Here, surgeons operate through a narrow port defined by a rigid bronchoscope. They currently tilt the head in order to aim the tip of the rigid bronchoscope at desired targets, which places large forces on the patient's mouth and neck. This forced tilting can cause complications including broken teeth and hyperextension of the neck [29], [30]. With a device like ours, procedures in deep, narrow cavities such as this could be accomplished with less forced tilting of rigid instruments.

In this study, we found that the force needed at the surgeon interface to deflect the tool with the static balance mechanism in place was low from the user's perspective. This can be understood by considering that there is a relatively long lever arm between the surgeon interface and the proximal elbow.

We note that with increased degrees of freedom comes the potential to increase dexterity, but at the cost of potentially increasing the complexity of the mental mapping for the physician. To assist with this, we envision a tool of this type typically being constrained at two points along its shaft, in order to fix the entry vector and thereby reduce the number of degrees of freedom that the physician must control.

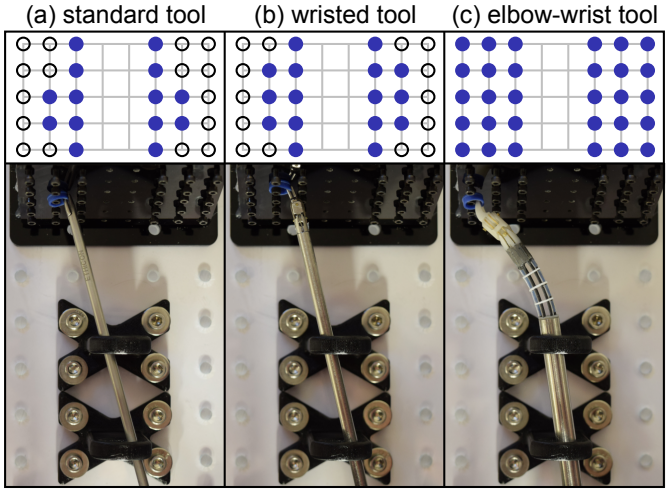

Fig. 9: Results of a peg transfer task through a lumen using (a) a standard laparoscopic tool with no additional wrist DOFs, (b) a laparoscopic tool with a distal wrist [6], and (c) the laparoscopic tool with both an elbow and wrist joint described in this paper. The user was instructed to move the ring from each peg to the corresponding mirror image peg on the other side of the board. Successful transfers are shown with a filled blue dot, while failed transfers are shown with a black ring.

IV. Discussion

The dexterous surgical tool presented here includes a mechanically actuated continuum section coupled with a wrist. This is the first example of a mechanically actuated multi-backbone section in a wristed fully mechanical surgical instrument. We have demonstrated that multi-backbone continuum joints, which typically are robotically actuated, can be statically balanced to reduce the forces required for manual operation in a hand-held device. We have also shown that the device improves a user's performance on the peg transfer task investigated in this work.

This tool utilizes a spring-gimbal static balance mechanism to generate torque in the opposite direction of the torque created by bending the elbows. The maximum required torque was 62.6% lower in the compensated configuration compared to the uncompensated configuration for the same deflection angle of 30°. Experiments demonstrated that the static balance mechanism reduces the required user actuation torque by an average of $0.16\,\mathrm{Nm}$ throughout the device's range of motion.

The shaft diameter and associated dimensions of this device were chosen for creating a proof-of-concept prototype, but this device could easily be downscaled if needed for a specific application. If downscaled, it is crucial that the smaller device maintain sufficient stiffness for clinical viability. To test this, we consider a prototype with a $5\,\mathrm{mm}$ diameter (half that of the current tool), and the same number of tubes and tube diameters, but simply smaller radial spacing. If we assume inextensible tubes, the theoretical stiffness of the downsized device will be very similar to that of the current prototype. This tool would theoretically deflect only about $0.7\,\mathrm{mm}$ for a force of $2.25\,\mathrm{N}$ (the peak force seen during suturing in [31]). As a result, it is likely that a downscaled device would be able to provide clinically reasonable force capability.

While the spring-gimbal approach was shown to be an effective static balance mechanism, its current form is likely too bulky for an operating room-ready medical device. The coaxial springs create a large overall tool diameter and would be challenging to sterilize. It will be useful in the future to reduce the size of the spring compensator. A variety of mechanisms could be investigated to provide the compensation force needed to statically balance the elbow, including a spring-cable mechanism routed over cams, which would generate a variable spring force (see also [32] and [33] for additional alternatives).

V. Conclusion

This tool has the potential to give surgeons high dexterity while performing challenging procedures in deep anatomical cavities such as in transoral or transanal applications. Overall, there is great potential for the use of more joints in a manual dexterous instrument to achieve similar levels of dexterity to that of robotic systems much less expensively. This prototype demonstrates the successful combination of multiple joints and a static balance mechanism. It illustrates that components typically associated solely with robotic systems can be incorporated in a non-robotic tool, bringing some of the advantages currently associated with surgical robotic systems to low-cost, hand-held devices.

References

[1] K. G. Cologne and A. J. Senagore, "Development of Minimally Invasive Colorectal Surgery: History, Evidence, Learning Curve, and Current Adaptation," in *Advanced Techniques in Minimally Invasive and Robotic Colorectal Surgery*. Springer US, 2015.

[2] M. J. Mack, "Minimally invasive and robotic surgery," *Jama*, vol. 285, no. 5, pp. 568–572, 2001.

[3] P. L. Anderson *et al.*, "Robot-like dexterity without computers and motors: a review of hand-held laparoscopic instruments with wrist-like tip articulation," *Expert Review of Medical Devices*, vol. 13, no. 7, pp. 661–672, 2016.

[4] M. Ongchin *et al.*, "Essentials and future directions of robotic pancreatic surgery," in *Essentials of Robotic Surgery*. Springer, 2015, pp. 131–148.

[5] R. M. Higgins *et al.*, "Cost analysis of robotic versus laparoscopic general surgery procedures," *Surgical endoscopy*, vol. 31, no. 1, pp. 185–192, 2017.

[6] P. L. Anderson *et al.*, "Comparing a Mechanical Analogue With the Da Vinci User Interface: Suturing at Challenging Angles," *IEEE Robotics and Automation Letters*, vol. 1, no. 2, pp. 1060–1065, 2016.

[7] N. Simaan *et al.*, "Design and Integration of a Telerobotic System for Minimally Invasive Surgery of the Throat," *The International Journal of Robotics Research*, vol. 28, no. 9, pp. 1134–1153, 2009.

[8] W. S. Ng *et al.*, "Development of a robotic colonoscope," *Digestive Endoscopy*, vol. 12, no. 2, pp. 131–135, 2000.

[9] K. Leibrandt *et al.*, "Effective Manipulation in Confined Spaces of Highly Articulated Robotic Instruments for Single Access Surgery," *IEEE Robotics and Automation Letters*, vol. 2, no. 3, pp. 1704–1711, 2017.

[10] C. Fan *et al.*, "Review of manual control methods for handheld maneuverable instruments," *Minimally Invasive Therapy & Allied Technologies*, vol. 22, no. 3, pp. 127–135, 2013.

[11] J. Diks *et al.*, "The mechanical master–slave manipulator: an instrument improving the performance in standardized tasks for endoscopic surgery," *Surgical endoscopy*, vol. 21, no. 6, pp. 1025–1031, 2007.

[12] F. Jelínek *et al.*, "Classification of Joints Used in Steerable Instruments for Minimally Invasive Surgery—A Review of the State of the Art," *Journal of Medical Devices*, vol. 9, no. 1, p. 010801, 2015.

[13] E. A. Arkenbout *et al.*, "A state of the art review and categorization of multi-branched instruments for NOTES and SILS," *Surgical Endoscopy*, vol. 29, no. 6, pp. 1281–1296, 2015.

[14] J. Catherine *et al.*, "Comparative review of endoscopic devices articulations technologies developed for minimally invasive medical procedures," *Applied Bionics and Biomechanics*, vol. 8, no. 2, pp. 151–171, 2011.

[15] F. Jelínek *et al.*, "Dragonflex smart steerable laparoscopic instrument," *Journal of medical devices*, vol. 8, no. 1, p. 015001, 2014.

[16] Bio-Inspired Technology Group, *TU Delft BITE Group*, 2018. [Online]. Available: https://www.bitegroup.nl/

[17] S. Awtar *et al.*, "Flexdex: a minimally invasive surgical tool with enhanced dexterity and intuitive control," *Journal of Medical Devices*, vol. 4, no. 3, p. 035003, 2010.

[18] G. Gerboni *et al.*, "Helixflex: bioinspired maneuverable instrument for skull base surgery," *Bioinspiration & biomimetics*, vol. 10, no. 6, p. 066013, 2015.

[19] J. Burgner-Kahrs *et al.*, "Continuum robots for medical applications: A survey," *IEEE Transactions on Robotics*, vol. 31, no. 6, pp. 1261–1280, 2015.

[20] N. Simaan, "Snake-Like Units Using Flexible Backbones and Actuation Redundancy for Enhanced Miniaturization," in *Proceedings of the 2005 IEEE International Conference on Robotics and Automation*. IEEE, 2005, pp. 3012–3017.

[21] N. Simaan *et al.*, "High dexterity snake-like robotic slaves for minimally invasive telesurgery of the upper airway," *Medical Image Computing and Computer-Assisted Intervention–MICCAI 2004*, pp. 17–24, 2004.

[22] K. M. Powell and M. I. Frecker, "Method for Optimization of a Nonlinear Static Balance Mechanism With Application to Ophthalmic Surgical Forceps," in *Volume 7: 29th Mechanisms and Robotics Conference, Parts A and B*, vol. 2005. ASME, 2005, pp. 441–447.

[23] J. Drenth and J. L. Herder, "Numerical Optimization of the Design of a Laparoscopic Grasper, Statically Balanced With Normal Springs," in *Volume 2: 28th Biennial Mechanisms and Robotics Conference, Parts A and B*. ASME, 2004, pp. 923–933.

[24] A. Stapel and J. L. Herder, "Feasibility Study of a Fully Compliant Statically Balanced Laparoscopic Grasper," in *Volume 2: 28th Biennial Mechanisms and Robotics Conference, Parts A and B*. ASME, 2004, pp. 635–643.

[25] S. Mattheis *et al.*, "Flex robotic system in transoral robotic surgery: the first 40 patients," *Head & neck*, vol. 39, no. 3, pp. 471–475, 2017.

[26] B. Seeliger *et al.*, "Enabling single-site laparoscopy: the sport platform," *Surgical endoscopy*, pp. 1–8, 2019.

[27] J. Shang *et al.*, "A single-port robotic system for transanal microsurgery-design and validation," *IEEE Robotics and Automation Letters*, vol. 2, no. 3, pp. 1510–1517, 2017.

[28] K. Xu and N. Simaan, "An investigation of the intrinsic force sensing capabilities of continuum robots," *IEEE Transactions on Robotics*, vol. 24, no. 3, pp. 576–587, 2008.

[29] D. L. Stahl *et al.*, "Complications of bronchoscopy: a concise synopsis," *International journal of critical illness and injury science*, vol. 5, no. 3, p. 189, 2015.

[30] F. Petrella *et al.*, "Operative rigid bronchoscopy: indications, basic techniques and results," *Multimed Man Cardiothorac Surg*, vol. 2014, pp. 1–6, 2014.
[31] J. Peirs *et al.*, "A micro optical force sensor for force feedback during minimally invasive robotic surgery," *Sensors and Actuators A: Physical*, vol. 115, no. 2-3, pp. 447–455, 2004.
[32] H. Hilpert, "Weight balancing of precision mechanical instruments," *Journal of Mechanisms*, vol. 3, no. 4, pp. 289–302, 1968.
[33] R. A. Lathrop, "Dexterity and guidance without automation: Surgical robot-like capabilities at a fraction of the cost," Ph.D. dissertation, Vanderbilt University, 2014.